Eur. Phys. J. B **51**, 345–355 (2006)
DOI: 10.1140/epjb/e2006-00243-5

THE EUROPEAN PHYSICAL JOURNAL B

Fully relativistic calculations of the $L_{2,3}$-edge XANES spectra for vanadium oxides

M.G. Brik[1,2,a], K. Ogasawara[1], H. Ikeno[3], and I. Tanaka[3]

[1] School of Science and Technology, Kwansei Gakuin University, 2-1 Gakuen, Sanda, Hyogo 669-1337, Japan
[2] Fukui Institute for Fundamental Chemistry, Kyoto University, 34-4, Takano-Nishihiraki-cho, Sakyo-ku, Kyoto 606-8103, Japan
[3] Department of Materials Science & Engineering, Kyoto University, Sakyo, Kyoto 606-8501, Japan

Received 9 March 2006
Published online 21 June 2006 –

Abstract. Fully relativistic multielectron method based on the numerical solution of the Dirac equation was used to calculate the $L_{2,3}$-edge X-ray absorption near edge structure (XANES) spectra of VO_2, V_2O_3, and V_2O_5 crystals. The key-points of the method are: i) usage of the molecular orbitals (MO); ii) absence of any fitting parameters; iii) wide area of application: to any ion in any symmetry; iv) possibility of numerical analysis of the MO composition. The calculated spectra are in a satisfactory agreement with experimental data available in the literature, including the absolute values of the transitions energy, the shape of the absorption bands, and polarization dependence. The assignment of the absorption bands in terms of the electronic configurations was done. The structure of the absorption bands is attributed to the splitting of the vanadium p- and d-orbitals; the magnitude of this splitting is estimated from the spectra. Covalency effects were considered for all hosts; it was shown that the contribution of the oxygen wave functions increases with increasing the vanadium oxidation state. Dependence of the relative positions of the vanadium $3d$ and oxygen $2p$ levels and energies of the "ligand–metal" charge transfer transitions on the vanadium oxidation state was analysed.

PACS. 78.70.Dm X-ray absorption spectra – 78.20.Bh Theory, models, and numerical simulation – 71.15.Rf Relativistic effects

1 Introduction

During last several decades, $3d$ transitional elements have been subjected to many thorough investigations due to their numerous applications. Among other experimental methods, X-ray absorption near edge structure (XANES) spectroscopy is a very powerful and versatile method of gaining knowledge about the electronic structure of the transitional metal ion. $L_{2,3}$ XANES spectra mainly correspond to the electric dipole transitions between the fully occupied $2p$-core levels and partially filled $3d$ electron shell. Coulomb and exchange interaction between $2p$ and $3d$ electrons give rise to structured XANES bands, detailed analysis of which can give information about the occupied and unoccupied states, energy levels splitting (caused by the spin-orbit interaction and crystal field), configuration interaction etc. Consistent theoretical modeling, in addition to the experimental studies, gives deeper insight into the X-ray absorption processes. First-principles (ab initio) calculations are of special importance since they help in revealing common and different features of the XANES spectra for various compounds.

First-principles calculations (in one-electron approximation) were proved successful in interpreting K-edge spectra [1–5]. Nevertheless, $L_{2,3}$ spectra can not be reproduced by these methods. An essential feature of the $L_{2,3}$ XANES spectra is that the correlation between $3d$ electrons together with $2p$ electrons and a hole within $2p$ states produces multiplet structure, which is impossible to obtain by one-electron calculations. Techniques to include the correlation between the $2p$ hole and excited electron were reported recently [6–9], but it should me emphasized that the multiplet structures were not computed at all. Another important aspect strongly affecting the shape of the $L_{2,3}$ XANES spectra is related to the interaction of the surrounding ions with $3d$ ion. Crystal-field atomic multiplet program based on the group theory formalism [10,11] incorporates the crystal (ligand) field effects. In spite of successful applications of this approach to transition-metal compounds, a number of adjustable parameters used in this method makes it impossible to apply it for an a priori analysis of the multiplet structures. Finally, both spin-orbit interaction (especially for $2p$

[a] e-mail: brik@fukui.kyoto-u.ac.jp; brik@ksc.kwansei.ac.jp

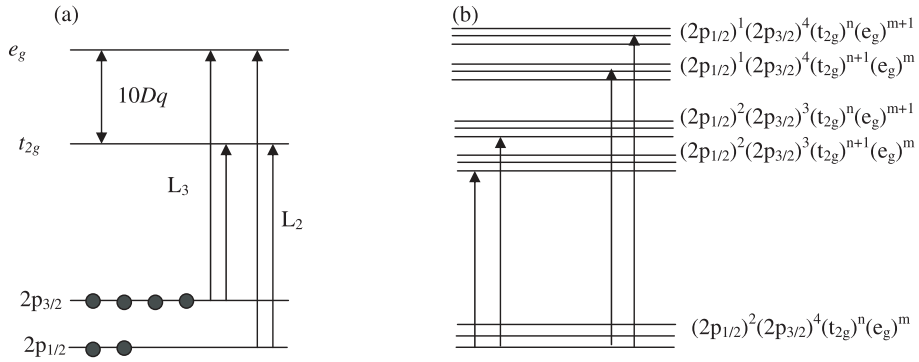

Fig. 1. Schematic representation of one-electron transitions corresponding to the L_2 and L_3 absorption bands in the XANES spectra; (a) – one-elecron picture; (b) – many-electron picture.

electrons) and covalent effects should be taken into account properly.

Schematically the processes leading to the formation of the $L_{2,3}$ XANES spectra are shown in Figure 1. In the octahedral crystal field the $3d$ orbitals split into t_{2g} and e_g orbitals with the former being the lower state and the latter being the higher with the energy separation of $10Dq$ (where Dq is referred to as the crystal field strength [12]). The $2p$ level is split by spin-orbit interaction into $2p_{1/2}$ and $2p_{3/2}$ (or L_2 and L_3, respectively) with the subscripts representing the quantum number of the total angular momentum. After absorbing an X-ray quantum, an electron from the $2p$ level is excited into t_{2g} or e_g states from $3d$ orbital. One-electron transitions between $2p$ and $3d$ states are shown in Figure 1 by vertical arrows. The energy separation between the L_2 and L_3 bands is mainly due to the spin-orbit splitting of $2p$-orbitals, whereas the structure of both L_2 and L_3 bands is caused by the crystal field splitting of $3d$ orbitals. Taking into account the degeneracy of all states involved into the transitions it is easy to show that the relative intensities for the L_3 absorption should be 6 and 4, and 3 and 2 for the L_2 absorption. If this were true, the XANES spectra for all elements would be the same, but this is, obviously, far from the real situation. It was demonstrated [13] that such one-electron consideration is insufficient to produce good agreement of the calculated spectra with experimental results, and more elaborated approach taking into account the interaction between the multiplets arising from all the possible electron configuration was proposed. It also was shown that the proper consideration of the multiplets interaction leads to the significant changes in the intensities ratio and significantly improves agreement between theory and experiment.

An approach which overcomes the above mentioned difficulties and combines the advantages of the fully relativistic first-principles methods with multiplet structure calculations and crystal field effect modeling has been recently developed by Ogasawara et al. [14]. In the present paper, this method is applied to the calculations and detailed analysis of the $L_{2,3}$-edge XANES spectra for VO_2, V_2O_3, V_2O_5 crystals. The chosen crystals form a series in which vanadium oxidation state changes as 3, 4, 5 in V_2O_3, VO_2, V_2O_5, respectively. In all these oxides vanadium ions occupy distorted octahedral positions, and it is interesting to see how the vanadium oxidation state influences XANES spectra and relative positions and properties of the vanadium $3d$ and oxygen $2p$ orbitals. The structure of the paper is as follows: in the next section we give the description of the method used in the present study. After having discussed the basic features of the computational procedure, we proceed with results of the calculations, and discussion.

2 Method of calculations

The discrete-variational multi-electron (DVME) method [14] is a configuration-interaction (CI) calculation program in which the four-component fully-relativistic molecular spinors obtained by the discrete-variational Dirac-Slater (DV-DS) cluster calculations [15] are used. The DVME method is based on the numerical solution of the Dirac equation, and its main advantages are as follows: 1) absence of any fitting parameters; 2) very wide area of applications: to any atom or ion in any symmetry from spherical to C_1 for any energy interval from IR to X-ray; 3) possibility to take into account all effects of chemical bonding formation and configuration interaction; 4) potential to calculate a wide variety of physical properties (such as transition probabilities, for example) using explicitly obtained wave functions. All relativistic effects are taken into account automatically. The key idea of the method is that the molecular orbitals (MO) are used throughout the calculations rather than atomic wave functions. This allows to perform the population analysis of the MO and assignment of the absorption bands in the calculated spectra in a straightforward way. Relativistic many-electron Hamiltonian is expressed as (in atomic units)

$$H = \sum_{i=1}^{n} \left[c\alpha \mathbf{p}_i + \beta c^2 - \sum_{\nu} \frac{Z_\nu}{|\mathbf{r}_i - \mathbf{R}_\nu|} + V_0(\mathbf{r}_i) \right] + \sum_{i=1}^{n} \sum_{j>i}^{n} \frac{1}{|\mathbf{r}_i - \mathbf{r}_j|} + \sum_{\mu} \frac{Z_\mu^{eff}}{|\mathbf{r}_i - \mathbf{R}_\mu|}, \quad (1)$$

where α, β are the Dirac matrices, c the velocity of light, $\mathbf{r}_i$, $\mathbf{p}_i$ the position and the momentum operator of the ith electron, Z_ν and $\mathbf{R}_\nu$ the charge and position of the υth nucleus, Z_μ^{eff} and $\mathbf{R}_\mu$ the effective charge and position of the μth ion outside the model cluster, n the number of explicitly treated electrons. $V_0(\mathbf{r}_i)$ is the potential from the other (core and valence) electrons [16]:

$$V_0 = \int \frac{\rho_0^G(\mathbf{r}')}{|\mathbf{r}-\mathbf{r}'|} d\mathbf{r}' + \frac{3}{4}\left[\frac{\rho^G(\mathbf{r})\, V_{xc}\left\{\rho^G(\mathbf{r})\right\} - \rho_0^G(\mathbf{r})\, V_{xc}\left\{\rho_0^G(\mathbf{r})\right\}}{\rho_1^G(\mathbf{r})} - V_{xc}\left\{\rho_1^G(\mathbf{r})\right\}\right], \quad (2)$$

where ρ^G, ρ_1^G, ρ_0^G represent the charge density of all electrons, that of explicitly treated electrons and that of the remaining electrons, respectively, and V_{xc} is the Slater's X_α potential. The superscript G indicates the ground state values. Diagonalization of the Hamiltonian (1) provides a complete electron energy level scheme (starting from the core electrons and ending up with open electron shells). Since the eigenfunctions are also obtained, the absorption spectra (for the electric dipole, electric quadrupole, magnetic dipole transitions) can be obtained in a straightforward manner after calculating appropriate matrix elements. For example, in the case of electric dipole transitions the oscillator strength (averaged over all possible polarizations) is calculated as follows:

$$I_{if} = \frac{2}{3}(E_f - E_i)\left|\left\langle \Psi_f \left| \sum_{k=1}^{n} \mathbf{r_k} \right| \Psi_i \right\rangle\right|^2, \quad (3)$$

Ψ_i and Ψ_f are the initial and final states with energies of E_i and E_f, respectively. In the case of the XANES spectra only those electrons occupying the molecular orbitals mainly composed of $2p$ and $3d$ states in the ground state are treated explicitly, since they are involved into the absorption transitions.

To emphasize the wide applicability of the method employed in the present paper and ensure the validity of the obtained results, we mention that it has been successfully applied to the analysis of the Cr^{4+} absorption spectrum in $Y_3Al_5O_{12}$ [17] and silicate crystals [18], $4f$–$4f$ absorption spectrum of $LiYF_4$:Dy^{3+} [19], $4f$–$5d$ absorption spectra of various trivalent lanthanides in $LiYF_4$ [20, 21], high lying energy $4f$ and $5d$ states of free trivalent lanthanides [22,23], calculations of the X-ray absorption near edge structure (XANES) spectra of transition metal ions [24–27], analysis of Cr^{3+} absorption spectra in $ZnAl_2S_4$ and $ZnGa_2O_4$ [28], covalence effects for Cr^{3+}, Mn^{4+}, Fe^{5+} in $SrTiO_3$ [29], analysis of the Eu^{3+} energy levels in LaF_3 [30].

Table 1. Distribution of electrons through the V^{4+} $2p$ and $3d$ orbitals in VO_2 ($3d^1$ open shell).

$2p_{1/2}$	$2p_{3/2}$	t_{2g}	e_g	Number of Slater determinants
Ground state configurations				
2	4	1	0	6
2	4	0	1	4
Excited configurations				
2	3	2	0	60
2	3	1	1	96
2	3	0	2	24
1	4	2	0	30
1	4	1	1	48
1	4	0	2	12

Table 2. Composition of 3d MO (in %) in VO_2.

	V^{4+} $3d$-orbitals	O^{2-} $2p$-orbitals	O^{2-} $2s$-orbitals
t_{2g} levels	96.9	3.1	0.00
	90.6	9.4	0.00
	90.2	9.8	0.00
e_g levels	83.1	14.2	2.6
	80.1	17.8	2.2
Averaged	88.2	10.8	1.0

3 Results of calculations and discussion

3.1 VO_2

Vanadium oxide VO_2 crystallizes in a monoclinic crystal structure (space group $P121/c1$ and lattice constants a = 5.7517 Å, b = 4.5378 Å, and c = 5.3825 Å [31]). There are four formula units per unit cell, and each V^{4+} ion is surrounded by six O^{2-} ions forming deformed octahedron. Among 7 electrons involved into the $L_{2,3}$-edge transitions, six occupy $2p$ states and 1 belongs to the $3d$ orbital. All possible electron configurations are listed below in Table 1.

The Hamiltonian (1) was diagonalized in the space spanned by 280 Slater determinants of the above configurations. The atomic orbitals used to form the MO were from $1s$ to $4p$ for vanadium and from $1s$ to $2p$ for oxygen (these orbitals were also used for other two oxides). $[VO_6]^{8-}$ cluster with the V^{4+}–O^{2-} bond lengths equal to 1.9022 Å (four bonds) and 1.95395 Å (two bonds) was used for the calculations; an influence of further crystal lattice ions was modeled by effective Madelung potential formed by point charges placed at the crystal lattice sites. To prove the necessity of using the MO, the Mulliken analysis [32] of the V^{4+} $3d$ orbitals was performed. The results of this analysis show that the contributions of the O^{2-} $2p$ states into the $3d$ MO can not be neglected (Tab. 2).

Experimental studies of the vanadium XANES spectra were reported recently in references [33,34]. The calculated XANES spectrum for VO_2 in comparison with experimental results [33] is shown in Figure 2 (oscillator strengths obtained by applying equation (3) were broadened by a Gaussian function for easier comparison with

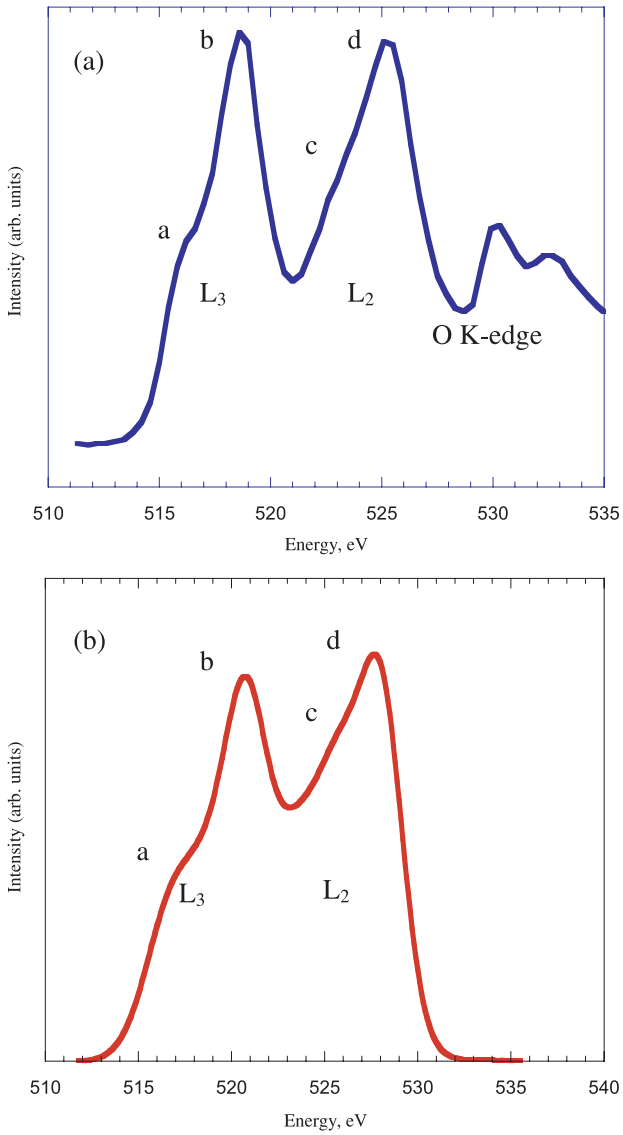

Fig. 2. VO_2 XANES spectra. (a) – experimental results [33]; (b) – calculated spectrum (this work).

experimental spectrum). As seen from Figure 2, there exists a good quantitative and qualitative agreement between both spectra (we note here that the oxygen K-edge has not been calculated in the present paper); the structure and shape of the L_2 and L_3 shapes are reproduced fairly well. Figure 3 shows the partial contribution from all six excited configurations listed in Table 1 to the theoretical spectrum in Figure 2. The $(2p_{1/2})^2(2p_{3/2})^3(t_{2g})^2(e_g)^0$ and $(2p_{1/2})^2(2p_{3/2})^3(t_{2g})^1(e_g)^1$ configurations give the dominant contribution to the peaks labeled as "a" and "b" in both calculated and experimental spectra. The peaks labeled as "c" and "d" arise from transitions from the ground state to the $(2p_{1/2})^1(2p_{3/2})^4(t_{2g})^2(e_g)^0$ and $(2p_{1/2})^1(2p_{3/2})^4(t_{2g})^1(e_g)^1$ electron configurations. It is interesting to note that the highest excited configuration $(2p_{1/2})^1(2p_{3/2})^4(t_{2g})^0(e_g)^2$ almost does not contribute to the spectrum. From both calculated and observed spectra one can estimate the spin-orbit splitting of the $2p$ state as the energy separation between the L_2 and L_3 bands to be about 8 eV and the crystal field strength $10Dq$ as the splitting of the L_2 and L_3 bands to be about 2 eV.

3.2 V_2O_3

V_2O_3 has a trigonal structure (space group *R-3cH* and lattice constants $a = 4.9537$ Å, $b = 4.9537$ Å, and $c = 14.0111$ Å [35]). There are six formula units per unit cell. 8 electrons involved into the $L_{2,3}$-edge transitions are distributed through the $2p$ states (six electrons) and $3d$ orbitals (2 electrons). All possible electron configurations are listed below in Table 3. 780 Slater determinants were used to construct the MO in the $[VO_6]^{9-}$ cluster with two different types of the V^{3+}–O^{2-} bond lengths: 1.9026 Å (three bonds) and 2.1685 Å (three bonds). Again, the Madelung potential effectively represents the influence of crystal lattice ions. Compositions of the $3d$ MO are shown in Table 4. The results of the XANES spectra calculations are shown in Figure 4. The number of electrons (and, therefore, the number of the multiplets) is greater in this case than in the previous; therefore, additional peaks appear in the spectrum. The shape of the spectrum is reproduced well, though there is a relatively small (1–2 eV) shift of the calculated spectrum with respect to the experimental towards higher energies. Such overestimation of the energy levels positions in the DVME calculations was reported earlier [22,23] and is an intrinsic feature of the method itself. In principle, this overestimation could be overcome by including high-lying states into the basis sets, but this would lead to a significant increase of the computational time. If the relative positions of the energy levels are more important (as in the case of the absorption spectrum calculations, when the differences between the pairs of the energy levels are of main interest), this overestimation can be left out of consideration [21].

Analysis of the partial contributions of the excited electron configurations to the calculated spectrum (Fig. 5) shows that the small peak "a" is due to the transition to the $(2p_{1/2})^2(2p_{3/2})^3\ (t_{2g})^3\ (e_g)^0$ configuration; peak "b" arises from the superposition of the $(2p_{1/2})^2(2p_{3/2})^3\ (t_{2g})^3\ (e_g)^0$ and $(2p_{1/2})^2(2p_{3/2})^3\ (t_{2g})^2\ (e_g)^1$ configurations. The most intensive peak "c" and a small peak "d" are mainly a superposition of two configurations: $(2p_{1/2})^2(2p_{3/2})^3\ (t_{2g})^2\ (e_g)^1$ and $(2p_{1/2})^2(2p_{3/2})^3\ (t_{2g})^1\ (e_g)^2$. Finally, four configurations $(2p_{1/2})^2(2p_{3/2})^3(t_{2g})^0(e_g)^3$, $(2p_{1/2})^1(2p_{3/2})^4\ (t_{2g})^3\ (e_g)^0$, $(2p_{1/2})^1(2p_{3/2})^4\ (t_{2g})^2\ (e_g)^1$, and $(2p_{1/2})^1(2p_{3/2})^4\ (t_{2g})^1\ (e_g)^2$ being mixed together produce two peaks "d" and "e". Again, like as in the previous case, the highest excited configuration $(2p_{1/2})^1(2p_{3/2})^4(t_{2g})^0(e_g)^3$ practically does not contribute to the calculated spectrum.

Polarized vanadium $L_{2,3}$ spectra in $(V_{0.988}Cr_{0.012})_2O_3$ (Fig. 6a) were reported in reference [36]. Figure 6b shows the calculated vanadium $L_{2,3}$ spectra for σ and π polarizations. All the trends in the experimental spectrum are confirmed by the theoretical calculations: the peak "d" at

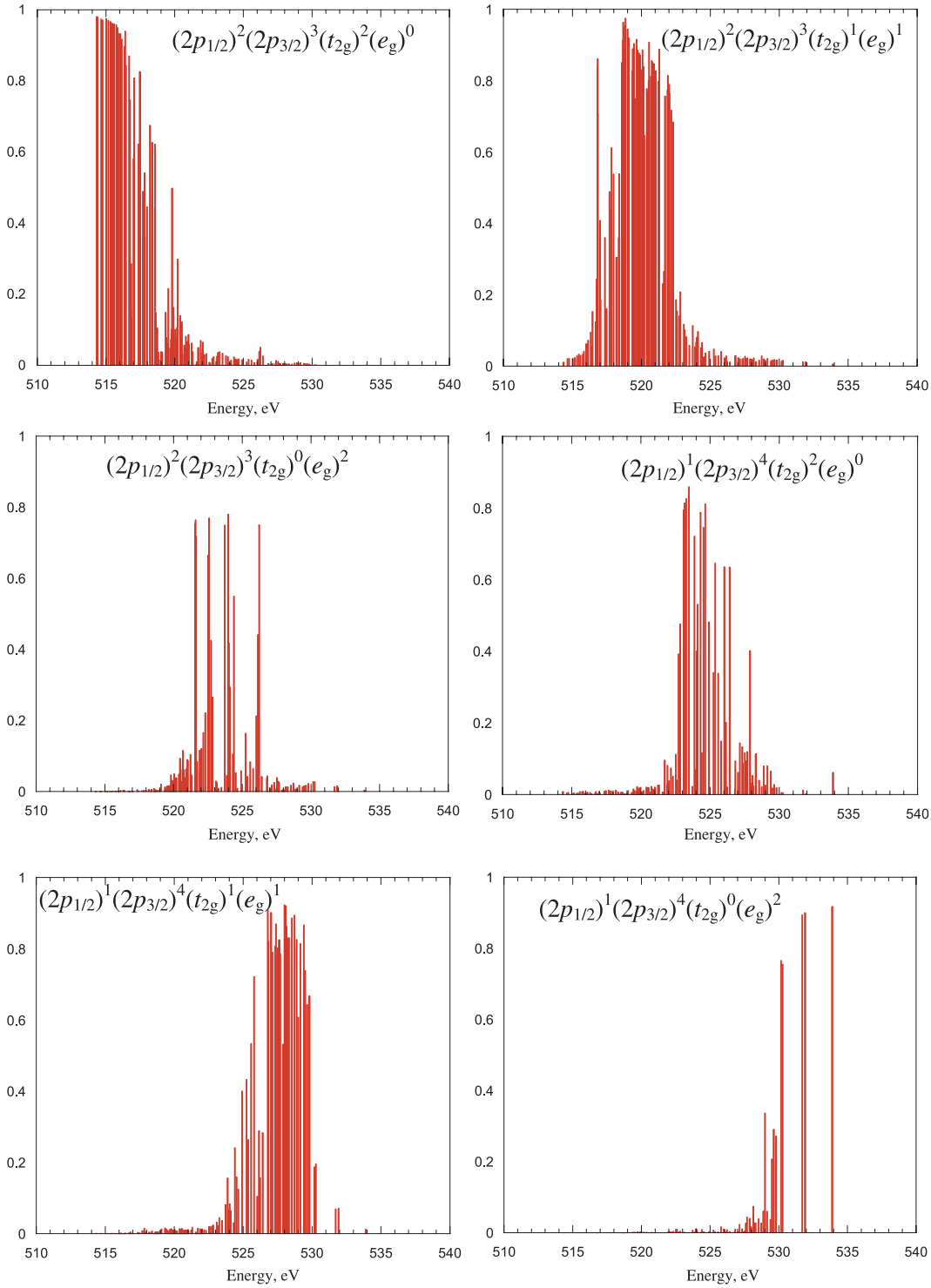

Fig. 3. Partial contributions of all excited configurations (Tab. 1) to the calculated VO_2 XANES spectrum.

around 520 eV is more intensive in π polarization then in σ; the peak "e" is more intensive than the peak "f" in π polarization, and less intensive then the peak "f" in σ polarization. The spin-orbit splitting of the $2p$ state as the energy separation between the L_2 and L_3 bands is about 8 eV and the crystal field strength $10Dq$ as the splitting of each L_2 and L_3 bands is about 2 eV.

3.3 V_2O_5

V_2O_5 crystallizes in the orthorhombic structure (space group $Pmmn$ and lattice parameters $a = 3.564$ Å, $b = 11.519$ Å, and $c = 4.373$ Å [37]. There are two formula units per unit cell. Since the oxidation state of vanadium ions is 5, there are no electrons in the $3d$ shell.

Table 3. Distribution of electrons through the V^{3+} $2p$ and $3d$ orbitals in V_2O_3 ($3d^2$ open shell).

$2p_{1/2}$	$2p_{3/2}$	t_{2g}	e_g	Number of Slater determinants
Ground state configurations				
2	4	2	0	30
2	4	1	1	24
2	4	0	2	6
Excited configurations				
2	3	3	0	80
2	3	2	1	240
2	3	1	2	144
2	3	0	3	16
1	4	3	0	40
1	4	2	1	120
1	4	1	2	72
1	4	0	3	8

Table 4. Composition of 3d MO (in %) in V_2O_3 (contribution from V^{3+} $4p$ orbitals is not shown).

	V^{3+} $3d$-orbitals	O^{2-} $2p$-orbitals	O^{2-} $2s$-orbitals
t_{2g} levels	94.7	5.1	0.00
	95.7	4.2	0.00
	95.6	4.3	0.00
e_g levels	85.6	11.6	1.5
	85.6	11.6	1.5
Averaged	91.4	7.4	0.6

There is only one ground state electron configuration and all excited configurations have only one electron which was promoted from one of the $2p$ orbitals. All possible electron configurations relevant to the XANES spectra in this case are listed in Table 5. The V^{5+}–O^{2-} bond lengths in the $[VO_6]^{7-}$ cluster are (all in Å) 1.5849, 1.7798, 1.8777, 2.0206 (two bonds), and 2.7845 Å. Variety of the bond lengths shows that the symmetry of this cluster is the lowest among all considered in the present paper. The contribution of the oxygen $2p$ and $2s$ orbitals to the $3d$ MO is shown in Table 6.

Diagonalization of the Hamiltonian (1) was performed n the space spanned by 61 Slater determinants composed of one-electron wave functions. Figure 7 shows the calculated XANES spectrum of V_2O_5 (lower part) in comparison with experimental spectrum [33] (upper part). Though agreement between both spectra in this case is worse than in previous ones (possibly, due to the low symmetry effects), we keep this example for the sake of completeness of this study. Besides, in the next section dependence of $3d$ orbital properties on the vanadium oxidation state will be considered for all three oxides studied in the present paper. Figure 8 shows the partial contributions of all excited configurations to the calculated spectrum. Additional peaks (to the left from the "a" peak in the calculated spectrum), which are not seen in the experiment, arise from the transitions from the ground state to the $(2p_{1/2})^2(2p_{3/2})^3$ $(t_{2g})^1$ $(e_g)^0$ and

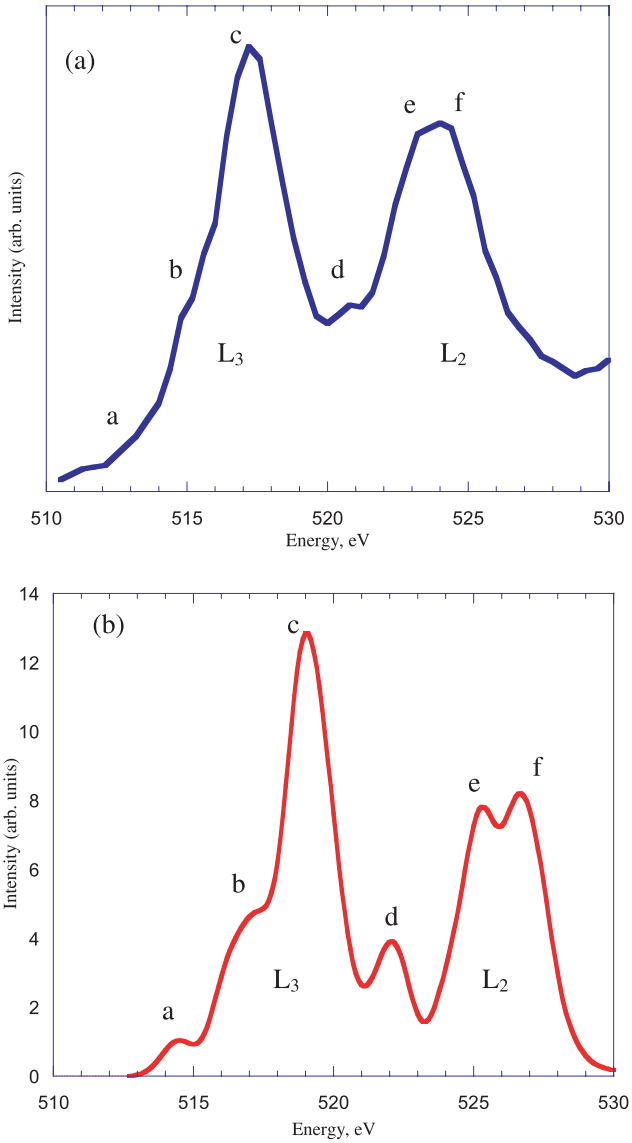

Fig. 4. V_2O_3 XANES spectra. (a) – experimental results [34]; (b) – calculated spectrum (this work).

$(2p_{1/2})^2(2p_{3/2})^3$ $(t_{2g})^0$ $(e_g)^1$configurations; they can be explained by the low-symmetry splitting of the multiplets corresponding to the above configurations. Peaks "a" and "b" at about 523 eV and 527 eV in the calculated spectrum are superpositions of contributions from two configurations: $(2p_{1/2})^2(2p_{3/2})^3$ $(t_{2g})^1$ $(e_g)^0$ and $(2p_{1/2})^1(2p_{3/2})^4$ $(t_{2g})^1$ $(e_g)^0$. The most intensive peak "c" at about 528 eV is due to the transitions from the ground electron configuration $(2p_{1/2})^2(2p_{3/2})^4$ $(t_{2g})^0$ $(e_g)^0$ to the $(2p_{1/2})^2(2p_{3/2})^3$ $(t_{2g})^0$ $(e_g)^1$ and $(2p_{1/2})^1(2p_{3/2})^4$ $(t_{2g})^0$ $(e_g)^1$ excited configurations. Finally, the peaks "d" and "e" at around 533 and 536 eV in the calculated spectrum arise from the $(2p_{1/2})^1(2p_{3/2})^4$ $(t_{2g})^1$ $(e_g)^0$ and $(2p_{1/2})^1(2p_{3/2})^4$ $(t_{2g})^0$ $(e_g)^1$ configurations. It is also interesting to note that all excited configurations in this case give rise to two clearly seen groups of lines, whereas in the above studied oxides each excited configuration gave one absorption band only.

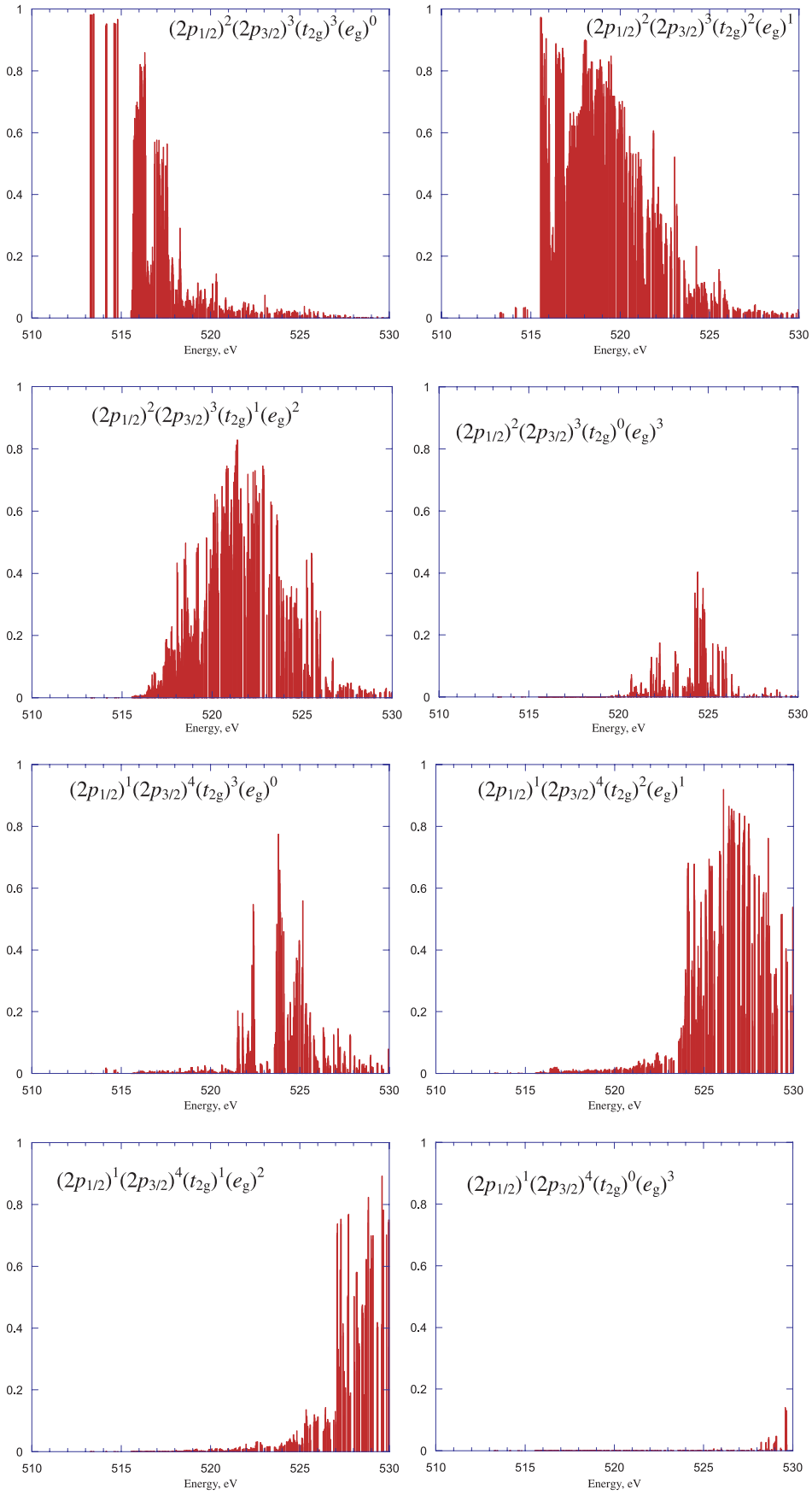

Fig. 5. Partial contributions of all excited configurations (Tab. 3) to the calculated V_2O_3 XANES spectrum.

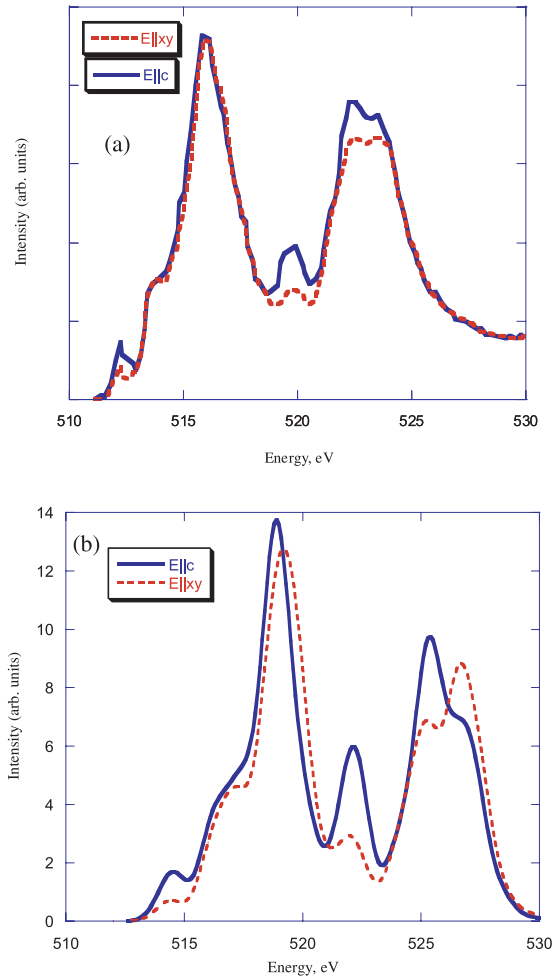

Fig. 6. Polarization-dependent V $L_{2,3}$ XANES spectra: (a) – experimental results [36]; (b) – calculated spectrum (this work).

The possible reason for that may lie in the electronic structure of the considered vanadium oxides. In VO_2 and V_2O_3 there are electrons in the 3*d* shell even in the ground configuration, whereas in V_2O_5 3*d* shell is unoccupied. In the first two oxides the Coulomb interaction between electrons within 3*d* orbital dominates the Coulomb interaction between 3*d* electrons and a hole in the 2*p* orbital, whereas in the last oxide V_2O_5 the Coulomb interaction between one electron in the 3*d* shell after the excitation and a hole in the 2*p* orbital is dominating.

One additional important issue is related to the structural peculiarities of V_2O_5 and choice of the cluster for calculations. A compound closely related to V_2O_5 is NaV_2O_5; the structure of both materials and the V–O distances are very similar. The formal valence states of vanadium and oxygen in NaV_2O_5 are "+4.5" and "–2", respectively; the structure of this crystal was reported in references [38,39]. It consists of the quasi-two-dimensional layers of VO_5 square pyramids separated by Na ions. The V–O–V rung unit is the basic unit of the electronic structure of this material [40]. It was shown in references [41,42] that very strong electron hybridization takes

Table 5. Distribution of electrons through the V^{5+} 2*p* and 3*d*orbitals in V_2O_5 ($3d^0$ open shell).

$2p_{1/2}$	$2p_{3/2}$	t_{2g}	e_g	Number of Slater determinants
Ground state configuration				
2	4	0	0	1
Excited configurations				
2	3	1	0	24
2	3	0	1	16
1	4	1	0	12
1	4	0	1	8

Table 6. Composition of 3d MO (in %) in V_2O_5 (small contribution from V^{5+} 3*p*, 4*p* orbitals is not shown).

	V^{5+} 3*d*-orbitals	O^{2-} 2*p*-orbitals	O^{2-} 2*s*-orbitals
t_{2g} levels	91.6	8.2	0.1
	74.8	24.6	0.5
	73.8	25.8	0.3
e_g levels	81.4	15.4	2.8
	67.6	24.9	1.0
Averaged	77.8	19.8	1.0

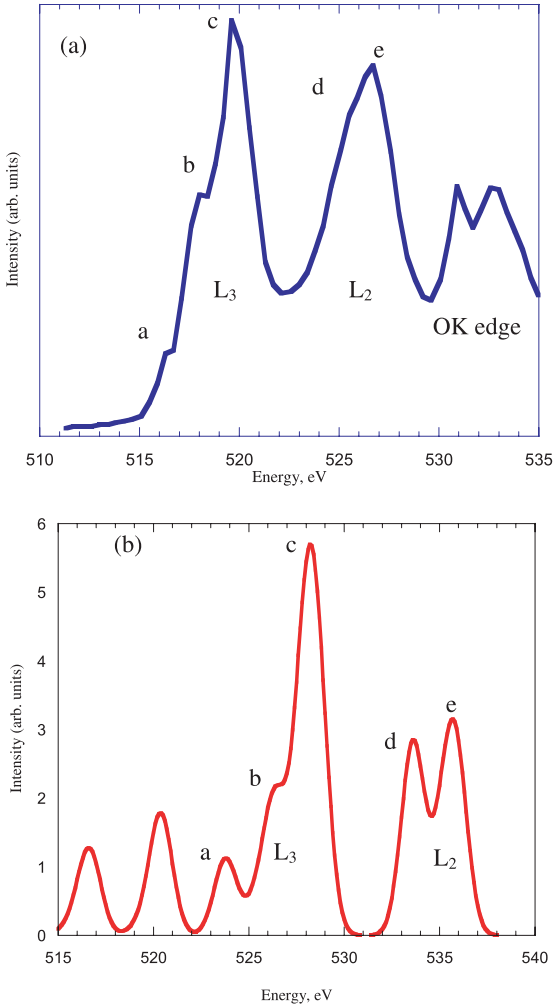

Fig. 7. V_2O_5 XANES spectra. (a) – experimental results [33]; (b) – calculated spectrum (this work).

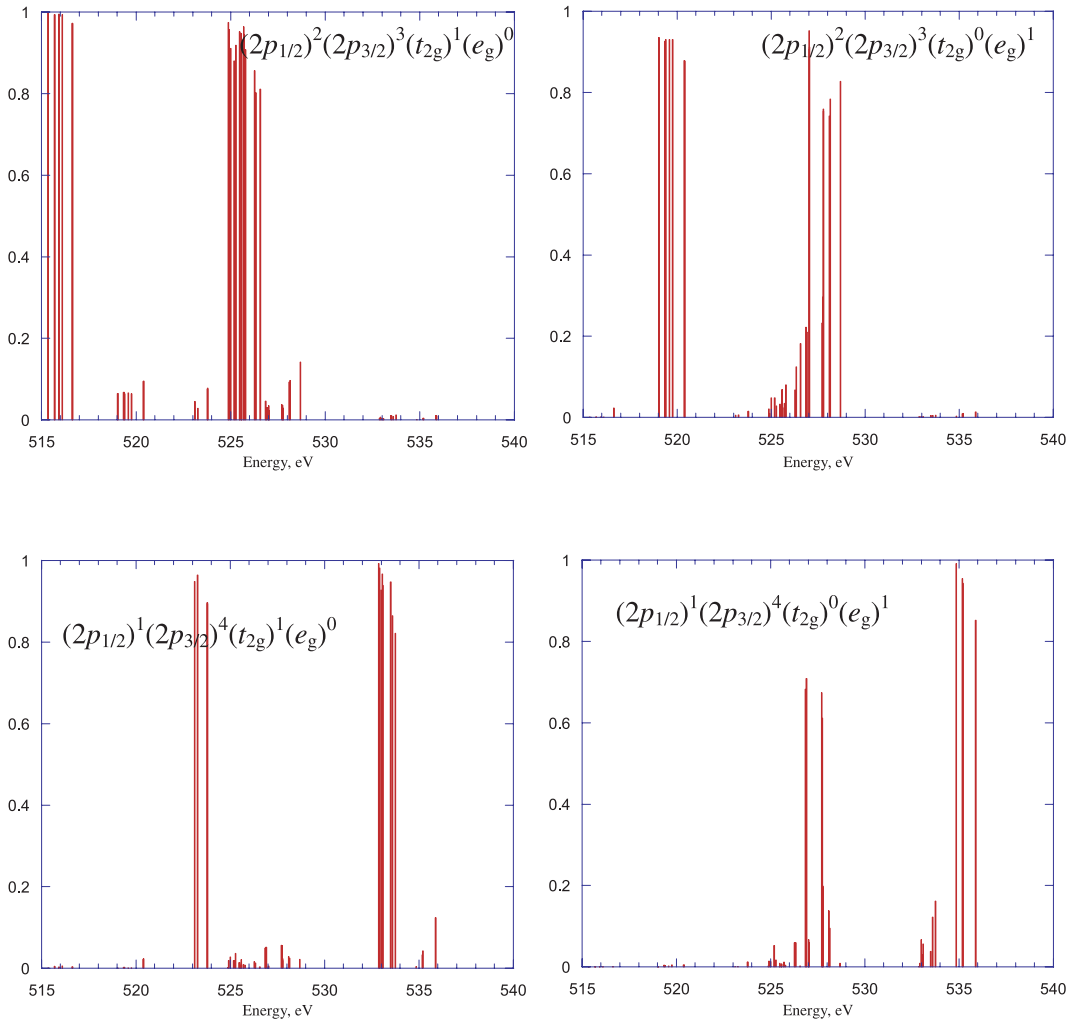

Fig. 8. Partial contributions of all excited configurations (Tab. 5) to the calculated V_2O_5 XANES spectrum.

place within this unit. Moreover, it leads to the formation of the V–O–V MO [41]. Results of the ab initio embedded-cluster calculations performed for a $[V_2O_9]$ by-pyramidal cluster [40] lead to the conclusion that the bridging oxygen ion in the V–O–V unit has the valence state "–1", but not "–2", as expected. In view of these remarks, it seems that a similar situation may take place in V_2O_5. If so, then the octahedral $[VO_6]$ cluster should be replaced by a larger one, to incorporate the V–O–V unit. Such calculations are in progress now.

4 Dependence of the vanadium 3d MO composition, their energies and the lowest "ligand-metal" charge transfer energies on the vanadium oxidation state

Comparison of data presented in Tables 2, 4, and 6 show that, first of all, the contributions of the oxygen atomic orbitals into the e_g MO is greater than into the t_{2g} MO. This is readily explained by the geometric properties of the considered clusters. In the octahedral cluster the t_{2g} orbitals are directed from the central ion into the space between the ligands, whereas the e_g orbitals are directed toward ligands. Therefore, the contribution of the ligands' wave functions should be greater in the latter case, as confirmed by the results of the Mulliken analyses.

Another interesting point is the contribution of the oxygen atomic orbitals as the function of the vanadium oxidation state. The valence of vanadium changes from "+3" in V_2O_3 to "+4" in VO_2 and "+5" in V_2O_5, and, at the same time, the averaged separation between vanadium and oxygen ions decreases in the same direction. The averaged contribution of the oxygen $2p$ orbitals into the $3d$ MO changes from 7.4% in V_2O_3 to 10.8% in VO_2 and 19.8% in V_2O_5. Therefore, an increase of the vanadium oxidation state together with decrease of the interionic separation is accompanied by an increase of the contributions of the ligands's wave function into the MO.

Figure 9 shows the energies of the $3d$ MO in all considered vanadium oxides. It is seen that as the oxidation state increases, the energies of the $3d$ MO monotonically decrease and low-symmetry splitting of the t_{2g} and e_g MO

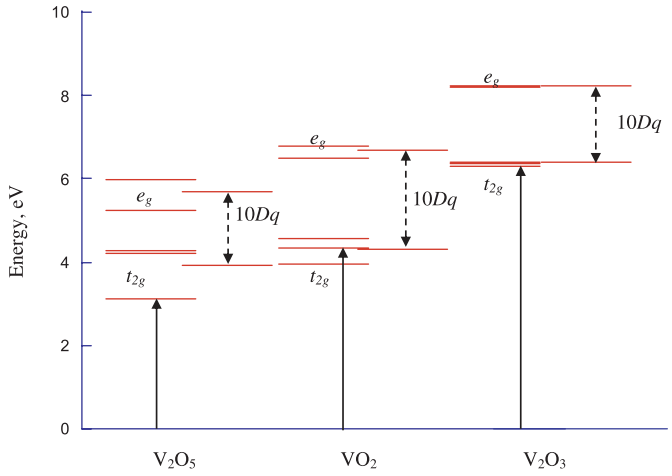

Fig. 9. Relative positions of the vanadium 3*d* levels in V_2O_5, VO_2, V_2O_3. Position of the highest oxygen 2*p* state is taken as zero in all compounds. Averaged energies for the group of the t_{2g} and e_g levels are also shown to the right from the corresponding levels (separation between these levels approximately corresponds to $10Dq$). "Oxygen–vanadium" charge transfer transitions with lowest energies are shown by vertical arrows.

monotonically increase. It is also instructive to note that the energies of the lowest "ligand-metal" charge transfer energies (when an electron is excited from the highest occupied oxygen 2*p* state into the lowest unoccupied vanadium 3*d* state forming a new vanadium state with electrical charge decreased by unity and maximum spin) also decrease when vanadium oxidation state increases. Estimation of these energies from our calculations yields the values 6.36 eV for V_2O_3 (in this case the oxygen 2*p* electron is excited into the highest t_{2g} orbital, since two lowest t_{2g} states are occupied by two *d* electrons of V^{3+} ion), 4.33 eV for VO_2 (in this case the oxygen 2*p* electron is excited into the second t_{2g} orbital, since the lowest t_{2g} state is occupied by one *d* electron of V^{4+} ion), and 3.14 eV for V_2O_5 (in this case the oxygen 2*p* electron is excited into the lowest t_{2g} orbital, since V^{5+} ion has no *d* electrons at all).

5 Conclusion

In the present paper the fully relativistic calculations of the vanadium $L_{2,3}$ XANES spectra in VO_2, V_2O_3, and V_2O_5 have been performed using recently developed first principles multi-electron method. Since the method is based on the solving the Dirac equation, all relativistic effects are considered automatically. Agreement between calculated and measured $L_{2,3}$ XANES spectra is good for VO_2 and V_2O_3 and worse for V_2O_5. The calculations not only reproduce the shape and relative intensities in the experimental spectra but give an unambiguous assignment of the absorption peaks in terms of the electronic configurations involved into the X-ray absorption. The partial contributions of all excited electron configurations to the calculated XANES spectra were determined and represented in a graphical way.

Introducing the MO concept allows to account for the covalence effects. The contribution of the oxygen 2*p* orbitals to the vanadium 3*d* orbitals increases with increasing the vanadium oxidation state. Significant contributions of the oxygen wave functions into the MO serve as a firm justification for using the MO scheme to get a reasonable description of the vanadium XANES spectra. From the calculations, the crystal field splitting of the vanadium 3*d* orbitals was found to be about 2–2.5 eV, and the spin-orbit splitting of the vanadium 2*p* orbitals was estimated as about 8–10 eV. Separation between vanadium 3*d* and oxygen 2*p* orbitals (and, as a consequence, oxygen-vanadium charge transfer energies) decreases with increasing vanadium oxidation state.

The present work was partially supported by following programs: i) the "Open Research Center" Project for Private Universities: matching fund subsidy from MEXT (Japanese Ministry of Education, Culture, Sports, Science and Technology), 2004–2008; and ii) Computational materials science unit in Kyoto University. K. Ogasawara was supported by the individual special research subsidy from Kwansei Gakuin University. We also thank the referee for bringing to our attention references [40–42].

References

1. J.J. Rehr, R.C. Albers, Rev. Mod. Phys. **72**, 621 (2000)
2. A. Filipponi, A. Di Cicco, C.R. Natoli, Phys. Rev. B **52**, 15122 (1995)
3. S.-D. Mo, W.Y. Ching, Phys. Rev. B **62**, 7901 (2000)
4. T. Mizoguchi, I. Tanaka, S. Yoshioka, M. Kunisu, T. Yamamoto, W.Y. Ching, Phys. Rev. B **70**, 045103 (2004)
5. T. Yamamoto, T. Mizoguchi, I. Tanaka, Phys. Rev. B **71**, 245113 (2005)
6. A.L. Ankudinov, A.I. Nesvizhskii, J.J. Rehr, Phys. Rev. B **67**, 115120 (2003)
7. P. Kruger, C.R. Natoli, Phys. Rev. B **70**, 245120 (2004)
8. S. Lazar, C. Hebert, H.W. Zandbergen, Ultramicroscopy **98**, 249 (2004)
9. P. Kruger, C.R. Natoli, J. Synchrotron Rad. **12**, 80 (2005)
10. F.M.F. de Groot, J. Electron Spectrosc. Relat. Phenom. **67**, 529 (1994)
11. F. de Groot, Chem. Rev. (Washington, D.C.) **101**, 1779 (2001)
12. S.Sugano, Y. Tanabe, H. Kamimura, *Multiplets of Transition-Metal Ions in Crystals* (Academic Press, New York and London, 1970)
13. H. Adachi, K. Ogasawara, Adv. Quant. Chem. **42**, 1 (2003)
14. K. Ogasawara, T. Iwata, Y. Koyama, T. Ishii, I. Tanaka, H. Adachi, Phys. Rev. B **64**, 115413 (2001)
15. A. Rosen, D.E. Ellis, H. Adachi, F.W. Averill, J. Chem. Phys. **65**, 3629 (1976)
16. S. Watanabe, H. Kamimura, Mater. Sci. Eng. B **3**, 313 (1989)

17. T. Ishii, K. Ogasawara, H. Adachi, I. Tanaka, J. Chem. Phys. **115**, 492 (2001)
18. T. Ishii, K. Fujimura, K. Ogasawara, H. Adachi, I. Tanaka, J. Phys.: Condens. Matter **13**, 5757 (2001)
19. M.G. Brik, T. Ishii, A.M. Tkachuk, S.E. Ivanova, I.K. Razumova, J. Alloys Compd. **374**, 63 (2004)
20. T. Ishii, K. Fujimura, K. Sato, M.G. Brik, K. Ogasawara, J. Alloys Compd. **374**, 18 (2004)
21. K. Ogasawara, S. Watanabe, H. Toyoshima, T. Ishii, M.G. Brik, H. Ikeno, I. Tanaka, J. Solid State Chem. **178**, 412 (2005)
22. K. Ogasawara, S. Watanabe, Y. Sakai, H. Toyoshima, T. Ishii, M.G. Brik, I. Tanaka, Jpn J. Appl. Phys. **43**, L611 (2004)
23. K. Ogasawara, S. Watanabe, T. Ishii, M.G. Brik, Jpn J. Appl. Phys. **44**, 7488 (2005)
24. K. Ogasawara, T. Miyamae, I. Tanaka, H. Adachi, Mater. Trans. **43**, 1435 (2002)
25. H. Ikeno, I. Tanaka, L. Miyamae, T. Mishima, H. Adachi, K. Ogasawara, Mater. Trans. **45**, 1414 (2004)
26. M.G. Brik, K. Ogasawara, T. Ishii, H. Ikeno, I. Tanaka, Rad. Phys. Chem. (accepted)
27. H. Ikeno, I. Tanaka, Y. Koyama, T. Mizoguchi, K. Ogasawara, Phys. Rev. B **72**, 075123 (2005)
28. M.G. Brik, Eur. Phys. J. B **49**, 269 (2006)
29. M.G. Brik, J. Phys. Chem. Solids **67**, 856 (2006)
30. M.G. Brik, I. Tanaka, T. Ishii, K. Ogasawara, A. Nakamura, S. Watanabe, J. Alloys Compd. **408–412**, 753 (2006)
31. J.M. Longo, P. Kierkegaard, Acta Chemica Scandinavica **24**, 420 (1970)
32. R.S. Mulliken, J. Chem. Phys. **23**, 1833 (1955)
33. R. Zimmermann, R. Claessen, F. Reinsert, P. Steiner, S. Hüfner, J. Phys.: Condens. Matter **10**, 5697 (1998)
34. A. Gloter, V. Serin, Ch. Turquat, C. Cesari, Ch. Leroux, G. Nihoul, Eur. Phys. J. B **22**, 179 (2001)
35. P. Rozier, A. Ratuszna, J. Galy, Zeit. Anorg. Allgem. Chemie **628**, 1236 (2002)
36. J.H. Park, L.H. Tjeng, A. Tanaka, J.W. Allen, C.T. Chen, P. Metcalf, J.M. Honig, F.M.F. de Croot, G.A. Sawatzky, Phys. Rev. B **61**, 11506 (2000)
37. W. Bystroem, K.A. Wilhelmi, O. Brotzen, Acta Chemica Scandinavica **4**, 1119 (1950)
38. A. Carpy, J. Galy, Acta Crystallogr. B **31**, 1481 (1975)
39. M. Isobe, Y. Udea, J. Phys. Soc. Jpn **65**, 1178 (1996)
40. L. Hozoi, C. Presura, C. de Graaf, R. Boer, Phys. Rev. B **67**, 035117 (2003)
41. H. Smolinski, C. Gros, W. Weber, U. Peuchert, G. Roth, M. Weiden, C. Geibel, Phys. Rev. Lett. **80**, 5164 (1998)
42. N. Suaud, M.-B. Lepetit, Phys. Rev. Lett. **88**, 056405 (2002)